LETTERS

Active terahertz metamaterial devices

Hou-Tong Chen[1]*, Willie J. Padilla[1]*†, Joshua M. O. Zide[2], Arthur C. Gossard[2], Antoinette J. Taylor[1] & Richard D. Averitt[1]†

The development of artificially structured electromagnetic materials, termed metamaterials, has led to the realization of phenomena that cannot be obtained with natural materials[1]. This is especially important for the technologically relevant terahertz (1 THz = 10^{12} Hz) frequency regime; many materials inherently do not respond to THz radiation, and the tools that are necessary to construct devices operating within this range—sources, lenses, switches, modulators and detectors—largely do not exist. Considerable efforts are underway to fill this 'THz gap' in view of the useful potential applications of THz radiation[2–7]. Moderate progress has been made in THz generation and detection[8]; THz quantum cascade lasers are a recent example[9]. However, techniques to control and manipulate THz waves are lagging behind. Here we demonstrate an active metamaterial device capable of efficient real-time control and manipulation of THz radiation. The device consists of an array of gold electric resonator elements (the metamaterial) fabricated on a semiconductor substrate. The metamaterial array and substrate together effectively form a Schottky diode, which enables modulation of THz transmission by 50 per cent, an order of magnitude improvement over existing devices[10].

A great deal of research into metamaterials has used microwave radiation; this is in part due to the ease of fabrication of sub-wavelength structures at these frequencies. Indeed, negative refractive index media[11,12] composed of negative permittivity[13] ($\varepsilon_1 < 0$) and negative permeability[14] ($\mu_1 < 0$) metamaterial elements was first demonstrated at microwave frequencies. This has led to intense theoretical, computational and experimental studies of exotic phenomena, such as perfect lensing[15] and cloaking[16,17]. Recently, researchers have ventured to create functional metamaterials at near-infrared and visible frequencies[18–20]. Considerably less work has concentrated on THz frequencies[21,22]. However, the design flexibility associated with metamaterials provides a promising approach, from a device perspective, towards filling the THz gap.

Metamaterials are geometrically scalable, which translates to operability over many decades of frequency. This engineering tunability is in fact a distinguishing and advantageous property of these materials. However, for many applications it is desirable to have real-time tunability. For instance, short-range wireless THz communication or ultrafast THz interconnects[23,24] require switches and modulators. Current state-of-the-art THz modulators based on semiconducting structures have the desirable property of being broadband, which is of relevance to THz interconnects, but are only able to modulate a few per cent[10] and usually require cryogenic temperatures[25]. Therefore, further improvement of the performance characteristics are required for practical applications. Here we present an efficient active metamaterial switch/modulator operating at THz frequencies. Although the modulation is based on a narrowband metamaterial resonance,

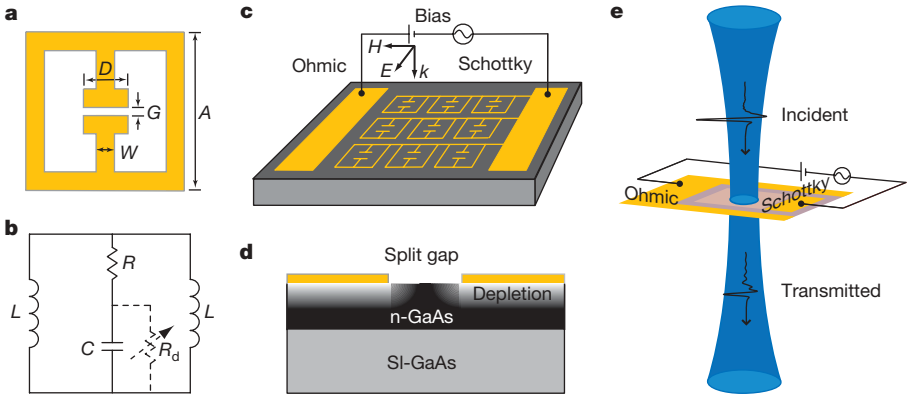

Figure 1 | Experimental design of the active THz metamaterial device. **a**, Geometry and dimensions of the THz metamaterial switch/modulator: $A = 36\ \mu m$, $G = 2\ \mu m$, $D = 10\ \mu m$ and $W = 4\ \mu m$. **b**, An equivalent circuit of the metamaterial element, where the dashed variable resistor corresponds to loss due to the substrate free carrier absorption within the split gap. **c**, The metamaterial elements are patterned with a period of 50 μm to form a planar array of $5 \times 5\ mm^2$. These elements are connected together with metal wires to serve as a metallic (Schottky) gate. A voltage bias applied between the Schottky and ohmic contacts controls the substrate charge carrier density near the split gaps, tuning the strength of the resonance. Orientation of the incident THz wave is indicated and the polarization of the electric field, *E*, magnetic field, *H*, and wave vector, *k*, are shown. **d**, Diagram of the substrate and the depletion region near the split gap, where the grey scale indicates the free charge carrier density. **e**, Experimental configuration for THz transmission measurements through a fabricated device. The black curves show the measured time-domain waveforms of the incident and transmitted THz pulses when a reverse gate voltage bias of 16 V is applied to the device and the THz electric field is polarized perpendicular to the connecting wires.

[1]Center for Integrated Nanotechnologies, Materials Physics & Applications Division, Los Alamos National Laboratory, Los Alamos, New Mexico 87545, USA. [2]Materials Department, University of California, Santa Barbara, California 93106, USA. †Present addresses: Department of Physics, Boston College, 140 Commonwealth Avenue, Chestnut Hill, Massachusetts 02467, USA (W.J.P.); Department of Physics, Boston University, 590 Commonwealth Avenue, Boston, Massachusetts 02215, USA (R.D.A.).
*These authors contributed equally to this work.

these devices can be engineered to operate at specific frequencies. This would enable, as an example, amplitude modulation of narrow-band devices, such as THz quantum cascade lasers, enabling near-term practical applications.

The metamaterial device used in this work is based on a recently presented electric analogue to split-ring resonators (SRRs)[26]. The geometry and dimensions are shown in Fig. 1a. The element consists of two single SRRs put together on the split gap side. These two rings provide inductances, L, and the split gap provides a capacitance, C, which are depicted as an equivalent circuit in Fig. 1b. A frequency-dependent dielectric resonant response results when it is patterned on a suitable substrate to form a planar periodic array of subwavelength structures. The two inductive loops are oppositely wound and thus any magnetic response is cancelled, resulting in a net electric response. The resistor R models the dissipation in the gold split rings, and the variable resistor R_d (shown dashed) models dissipation due to the substrate free carrier absorption within the split gap[27].

In our device, the metamaterial elements are electrically connected using conducting wires such that the entire metamaterial array functions as a voltage gate, schematically depicted in Fig. 1c. This structure has been designed to enable voltage control of the conductivity of the substrate at the split gaps, thereby controlling the THz transmission. The substrate consists of a 1-μm-thick n-type gallium arsenide (GaAs) layer with a free electron density of $n = 1.9 \times 10^{16}\,\mathrm{cm}^{-3}$ grown on a semi-insulating gallium arsenide (SI-GaAs) wafer by molecular beam epitaxy (MBE), as detailed in Fig. 1d. The ohmic contact is fabricated by electron-beam deposition of 20 nm of nickel, 20 nm of germanium, and 150 nm of gold in sequence, followed by rapid thermal annealing at 350 °C for 1 min in a nitrogen atmosphere. Next, the planar electric resonator array is fabricated using conventional photolithography and electron-beam deposition of a 10-nm-thick adhesion layer of titanium on the GaAs substrate, followed by 200 nm of gold. The metal and n-GaAs form a Schottky junction and the connected metamaterial resonators serve as a metallic gate. Current–voltage (I–V) measurements confirm the Schottky character of the device (Supplementary Fig. 1).

Terahertz time-domain spectroscopy (THz-TDS)[28] was used to characterize the performance of the metamaterial device, and has been described elsewhere in detail[29]. In our photoconductive THz-TDS experiment, a polyethylene lens focuses the linearly polarized THz beam onto the metamaterial sample to a diameter of about 3 mm, and a second polyethylene lens recollimates the transmitted THz beam, which is directed to a photoconductive receiver. The experiments were performed at room temperature in a dry air atmosphere. In THz-TDS, the time-varying electric field of the impulsive THz radiation is recorded, and the electric field spectral amplitude and phase are directly obtained by performing Fourier analysis. Measurements of the metamaterial device with respect to a suitable reference, as illustrated in Fig. 1e, allow determination of the complex transmission as a function of frequency, $\tilde{t}(\omega)$. Inversion of $\tilde{t}(\omega)$ further permits model-independent calculation of the frequency-dependent complex permittivity[28], $\tilde{\varepsilon}(\omega) = \varepsilon_1(\omega) + i\varepsilon_2(\omega)$, where ε_1 and ε_2 are the real and imaginary portions, respectively.

All experiments were performed at normal incidence, with the THz magnetic field lying completely in-plane. The polarization of the THz electric field was either perpendicular or parallel to the split gaps (and connecting wires). The wires connecting the individual electric resonators are necessary (as described above) to provide electrical connectivity to the gate. Importantly, these connecting wires have little effect on the electromagnetic properties of the electric resonators when the THz electric field is normal to the connecting wires. This was confirmed by finite element simulations using commercial software, as shown in Fig. 2a and b. The electric field is strongly concentrated at the split gaps, and there is no significant surface current flowing along the connecting metal wires between electric resonators at the resonant frequency (~0.72 THz).

Without an applied gate bias, the device is not expected to display resonant behaviour associated with the electric resonators because the substrate free charge carriers short out the capacitive response associated with the gaps. Upon application of a voltage, a resonant transmission should result as carriers in the substrate are displaced from the gaps. The blue curve in Fig. 2c shows the frequency-dependent transmitted intensity at a reverse gate bias of 16 V, where the polarization of the incident THz electric field is perpendicular to the connecting wires. Two distinct resonances are observed. The 0.72 THz resonance is the LC response associated with circulating currents in each metamaterial element, while the resonance at 1.65 THz is due to in-phase dipolar currents along the 36 μm lengths of the elements[22]. The spectrum is consistent with that from the same structure fabricated on an SI-GaAs substrate with no free carriers (red curve) and with simulation (black dashed curve), as shown in Fig. 2c. In Fig. 2d the real permittivity $\varepsilon_1(\omega)$ of the THz metamaterial devices is shown as extracted from the experimental data of Fig. 2c assuming a cubic unit cell[26].

The resonances are strongly dependent on gate bias, as shown in Fig. 3. With zero applied voltage to the gate (black curves), the metamaterial response is very weak and does not show significant

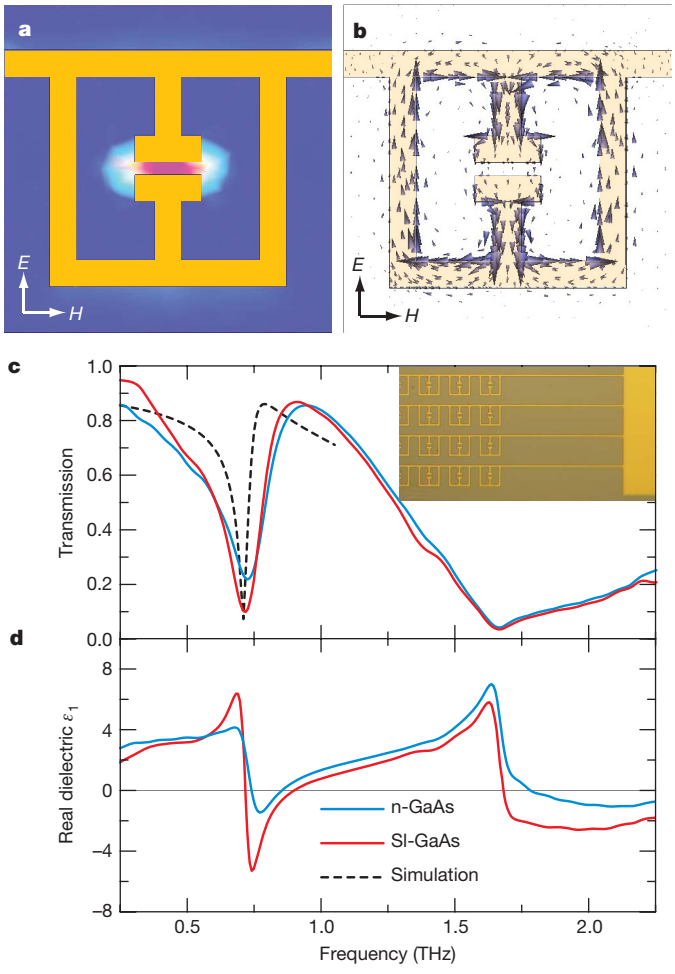

Figure 2 | Simulated and experimental characterization of THz metamaterial devices. **a**, Simulated norm of the electric field, $|\boldsymbol{E}|$, and **b**, the surface current density of a metamaterial element at the 0.72 THz resonance. **c**, Frequency dependent transmitted intensity of THz radiation, and **d**, the corresponding extracted real part of the effective permittivity of the voltage controlled metamaterial device at 16 V reverse gate bias (blue curves) and the same structure fabricated on an SI-GaAs substrate (red curves). The dashed black curve is the simulated transmission for a device on the SI-GaAs substrate. The inset to **c** shows a photograph of the individual resonant elements, connecting wires and the contact pad, which together form the Schottky gate of the metamaterial device.

frequency dependence near the 0.72 THz resonance, as the relatively conductive substrate shorts the capacitive split gap and no *LC* resonance can be established. An increasing reverse gate bias depletes an increasing fraction of electrons in the n-GaAs layer near the metallic gate, thus significantly reducing the conductivity of the substrate near the split gaps, thereby restoring the *LC* resonant response. This is verified by the experimental results shown in Fig. 3a, as the resonances in the transmission spectra narrow and increase in amplitude with increasing reverse bias. At a reverse gate bias of 16 V, a 50% relative intensity change of transmission is observed at 0.72 THz, making this device a reasonably efficient narrowband THz switch/modulator. We note that the transmitted intensity of the 1.65 THz resonance also decreases with bias. This is because the substrate carriers screen the dipolar currents and is not associated with shorting of the capacitive gap of the metamaterial elements. Figure 3b shows the corresponding permittivity $\varepsilon_1(\omega)$ of the metamaterial device at various gate biases. Clearly, $\varepsilon_1(\omega)$ of the device is significantly modified by the applied gate bias. $\varepsilon_1(\omega)$ increases on the low frequency side of the resonance while at higher frequencies it decreases to less than unity and even becomes negative.

From Fig. 3a, it is evident that at frequencies (~1 THz) between the two resonances, the transmission is significantly enhanced as a function of reverse gate bias. We have investigated whether this enhancement arises from a reduction of free carrier absorption in the n-GaAs layer due to depletion. For this purpose, we fabricated a device without the metamaterial array—only the connecting wires remained as the Schottky contact. With the same polarization of the THz electric field, that is, perpendicular to the connecting wires as indicated by the inset to Fig. 3c, we measured its THz transmission at various bias voltages. As shown in Fig. 3c for reverse biases of 0 and 16 V, the change of THz transmission is hardly observable and variations are within the experimental noise. Additionally, we performed measurements of the free carrier absorption in the n-GaAs layer using an unpatterned sample with SI-GaAs as the reference. The relative intensity change of transmission between samples with carrier density $n = 1.9 \times 10^{16}\,\mathrm{cm}^{-3}$ and $n \approx 0$ is less than 10% at ~1 THz. Furthermore, in our metamaterial device only a small fraction of the n-GaAs layer is depleted by the reverse gate bias and thus the reduction of free carrier absorption is not nearly enough to account for the change in transmission in Fig. 3a. The transmission enhancement in this frequency range is dominated by the metamaterial structure and is largest in the vicinity where $\varepsilon_1(\omega) \approx 1$.

This active metamaterial device was designed such that the *LC* resonant response occurs with the electric field polarized perpendicular to the connecting wires. This eliminates the Drude-like response that occurs when the THz electric field is parallel to the array of connecting wires[13]. Nonetheless, with the electric field applied parallel to the connecting wires, a response that changes with applied bias is still observed, as shown in Fig. 4a. The small transmitted intensity at low frequencies results from the Drude-like response of the connecting wires. Superimposed on this is a resonance at 1.25 THz from the metamaterial elements. This resonant response is associated with dipolar currents in the elements analogous to the higher-lying resonance when the electric field is perpendicular to the connecting wires. As such, the variation in $\varepsilon_1(\omega)$ shown in Fig. 4b

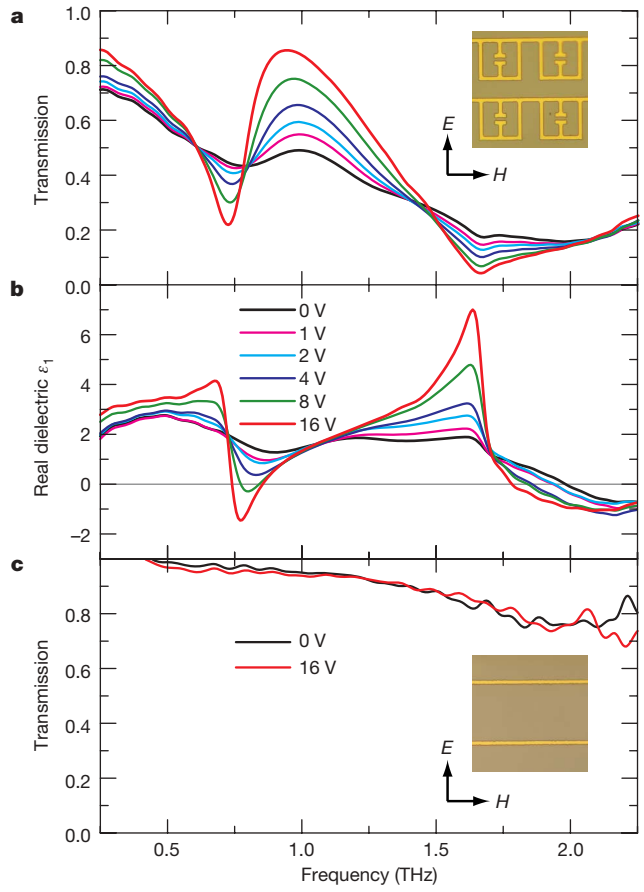

Figure 3 | Switching performance of the active THz metamaterial device as a function of gate voltage bias with the polarization of the THz electric field perpendicular to the connecting wires. **a**, Frequency-dependent transmitted intensity of THz radiation, and **b**, the corresponding permittivity for various reverse gate biases. **c**, THz transmission through a device with metamaterials removed, at reverse biases of 0 and 16 V. The insets show the polarization configuration of the THz electric and magnetic fields.

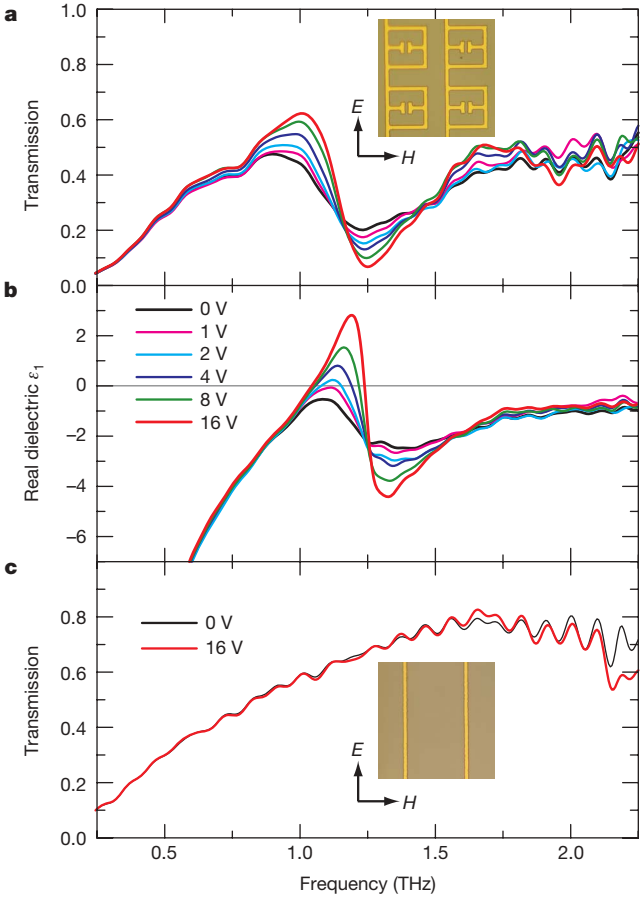

Figure 4 | Switching performance of the active THz metamaterial device as a function of gate voltage bias with the polarization of the THz electric field parallel to the connecting wires. **a–c**, As Fig. 3 but with the polarization of the THz electric field parallel to the connecting wires.

arises from substrate carriers screening the dipolar currents. An applied bias depletes the carriers, thus restoring the dipolar resonant response. Figure 4c shows the response for an array of parallel wires as the Schottky contact to the n-type substrate without the metamaterial elements. As expected, only a Drude-like response associated with the wires is observed. Thus without the resonant metamaterial elements and their critical dependence upon substrate properties, it is not possible to modulate the transmission with an applied bias. This further confirms the importance of the metamaterial elements in creating active THz devices.

Substrates typically used to fabricate planar metamaterial structures (for example, Si, GaAs, Teflon) are insulators and are essentially lossless at THz frequencies. In this case, the metamaterial structure and the substrate can be modelled as an equivalent *LCR* resonant circuit as shown in Fig. 1b without the variable resistor R_d. However, when the substrate is lossy (in our case this is a result of doping), the finite resistance at the split gap has to be considered. The equivalent circuit should be modified by attaching a variable resistor in parallel to the capacitor[27]. In our device, the gate bias changes this resistance by depleting the free charge carriers and modifies the resonance strength. The fact that there are no significant shifts of the resonance frequencies indicates that the magnitude of the capacitance at the split gap is not strongly affected by the applied gate bias—rather, the capacitance is shunted.

Although the metamaterial structure presented here is a first generation device (that is, no optimization has been attempted), the performance as a THz modulator already exceeds current state-of-the-art electrical THz modulators—based on semiconductor structures[10]—by one order of magnitude on resonance, and operates at room temperature. Higher modulation efficiency for practical applications is expected to be achievable through device optimization, that is, by varying the doping concentration and/or the thickness of the doping layer. One problem with the current design is that high frequency modulation is not possible. We performed measurements of the THz intensity as a function of modulation frequency by applying a rectangular a.c. reverse gate bias alternating between 0 and 16 V. The large area ($5 \times 5\,mm^2$) of the metamaterial array results in a large overall device capacitance, yielding a maximum modulation frequency of several kilohertz (Supplementary Fig. 2). We anticipate significant increases in the modulation frequency from reducing the total capacitance and resistance of the device by, for example, patterning the n-GaAs regions of the substrate and/or using interdigitated contacts.

This demonstration of an active metamaterial device relied on electrically connecting the individual metamaterial elements. It is important to emphasize that this does not compromise the resonant *LC* response of the elements, and thereby provides additional design flexibility for metamaterials in general. The approach presented here for active THz metamaterials naturally extends to magnetically resonant metamaterials. Finally, consideration of the substrate or embedding environment also offers considerable flexibility in the design of active metamaterial devices at any frequency range.

Received 3 July; accepted 10 October 2006.

1. Veselago, V. G. The electrodynamics of substances with simultaneously negative values of ε and μ. *Sov. Phys. Usp.* **10,** 509–514 (1968).
2. Oliveira, F. *et al.* Neural network analysis of terahertz spectra of explosives and bio-agents. *Proc. SPIE* **5070,** 60–70 (2003).
3. Zimdars, D. Fiber-pigtailed terahertz time domain spectroscopy instrumentation for package inspection and security imaging. *Proc. SPIE* **5070,** 108–116 (2003).
4. Federici, J. F. *et al.* THz imaging and sensing for security applications—explosives, weapons and drugs. *Semicond. Sci. Technol.* **20,** S266–S280 (2005).
5. Barber, J. *et al.* Temperature-dependent far-infrared spectra of single crystals of high explosives using terahertz time-domain spectroscopy. *J. Phys. Chem. A* **109,** 3501–3505 (2005).
6. Liu, H-B., Chen, Y., Bastiaans, G. J. & Zhang, X-C. Detection and identification of explosive RDX by THz diffuse reflection spectroscopy. *Opt. Express* **14,** 415–423 (2006).
7. Kawase, K., Ogawa, Y., Watanabe, Y. & Inoue, H. Non-destructive terahertz imaging of illicit drugs using spectral fingerprints. *Opt. Express* **11,** 2549–2554 (2003).
8. Ferguson, B. & Zhang, X-C. Materials for terahertz science and technology. *Nature Mater.* **1,** 26–33 (2002).
9. Köhler, R. *et al.* Terahertz semiconductor-heterostructure laser. *Nature* **417,** 156–159 (2002).
10. Kleine-Ostmann, T., Dawson, P., Pierz, K., Hein, G. & Koch, M. Room-temperature operation of an electrically driven terahertz modulator. *Appl. Phys. Lett.* **84,** 3555–3557 (2004).
11. Smith, D. R., Padilla, W. J., Vier, D. C., Nemat-Nasser, S. C. & Schultz, S. Composite medium with simultaneously negative permeability and permittivity. *Phys. Rev. Lett.* **84,** 4184–4187 (2000).
12. Shelby, R. A., Smith, D. R. & Schultz, S. Experimental verification of a negative index of refraction. *Science* **292,** 77–79 (2001).
13. Pendry, J. B., Holden, A. J., Stewart, W. J. & Youngs, I. Extremely low frequency plasmons in metallic mesostructures. *Phys. Rev. Lett.* **76,** 4773–4776 (1996).
14. Pendry, J. B., Holden, A. J., Robbins, D. J. & Stewart, W. J. Magnetism from conductors and enhanced nonlinear phenomena. *IEEE Trans. Microwave Theory Tech.* **47,** 2075–2084 (1999).
15. Pendry, J. B. Negative refraction makes a perfect lens. *Phys. Rev. Lett.* **85,** 3966–3969 (2000).
16. Pendry, J. B., Schurig, D. & Smith, D. R. Controlling electromagnetic fields. *Science* **312,** 1780–1782 (2006).
17. Leonhardt, U. Optical conformal mapping. *Science* **312,** 1777–1780 (2006).
18. Zhang, S. *et al.* Experimental demonstration of near-infrared negative-index metamaterials. *Phys. Rev. Lett.* **95,** 137404 (2005).
19. Zhou, J. *et al.* Saturation of the magnetic response of split-ring resonators at optical frequencies. *Phys. Rev. Lett.* **95,** 223902 (2005).
20. Grigorenko, A. N. *et al.* Nanofabricated media with negative permeability at visible frequencies. *Nature* **438,** 335–338 (2005).
21. Yen, T. J. *et al.* Terahertz magnetic response from artificial materials. *Science* **303,** 1494–1496 (2004).
22. Padilla, W. J., Taylor, A. J., Highstrete, C., Lee, M. & Averitt, R. D. Dynamical electric and magnetic metamaterial response at terahertz frequencies. *Phys. Rev. Lett.* **96,** 107401 (2006).
23. Wang, K. & Mittleman, D. M. Metal wires for terahertz wave guiding. *Nature* **432,** 376–379 (2004).
24. Mendis, R. & Grischkowsky, D. THz interconnect with low-loss and low-group velocity dispersion. *IEEE Microwave Wireless Compon. Lett.* **11,** 444–446 (2001).
25. Kersting, R., Strasser, G. & Unterrainer, K. Terahertz phase modulator. *Electron. Lett.* **36,** 1156–1158 (2000).
26. Schurig, D., Mock, J. J. & Smith, D. R. Electric-field-coupled resonators for negative permittivity metamaterials. *Appl. Phys. Lett.* **88,** 041109 (2006).
27. Ikonen, P. & Tretyakov, S. Generalized permeability function and field energy density in artificial magnetics. Preprint at ⟨http://arxiv.org/abs/physics/0602182⟩ (2006).
28. Grischkowsky, D., Keiding, S., van Exter, M. & Fattinger, Ch Far-infrared time-domain spectroscopy with terahertz beams of dielectrics and semiconductors. *J. Opt. Soc. Am. B* **7,** 2006–2015 (1990).
29. O'Hara, J. F., Zide, J. M. O., Gossard, A. C., Taylor, A. J. & Averitt, R. D. Enhanced terahertz detection via ErAs:GaAs nanoisland superlattices. *Appl. Phys. Lett.* **88,** 251119 (2006).

Supplementary Information is linked to the online version of the paper at www.nature.com/nature.

Acknowledgements We acknowledge support from the Los Alamos National Laboratory LDRD programme, and from the Center for Integrated Nanotechnologies.

Author Information Reprints and permissions information is available at www.nature.com/reprints. The authors declare no competing financial interests. Correspondence and requests for materials should be addressed to H.-T.C. (chenht@lanl.gov).